

*Atmospheric drivers of sea-level
fluctuations and nuisance floods along the
mid-Atlantic coast of the USA*

**Scott C. Sheridan, Douglas
E. Pirhalla, Cameron C. Lee & Varis
Ransibrahmanakul**

Regional Environmental Change

ISSN 1436-3798

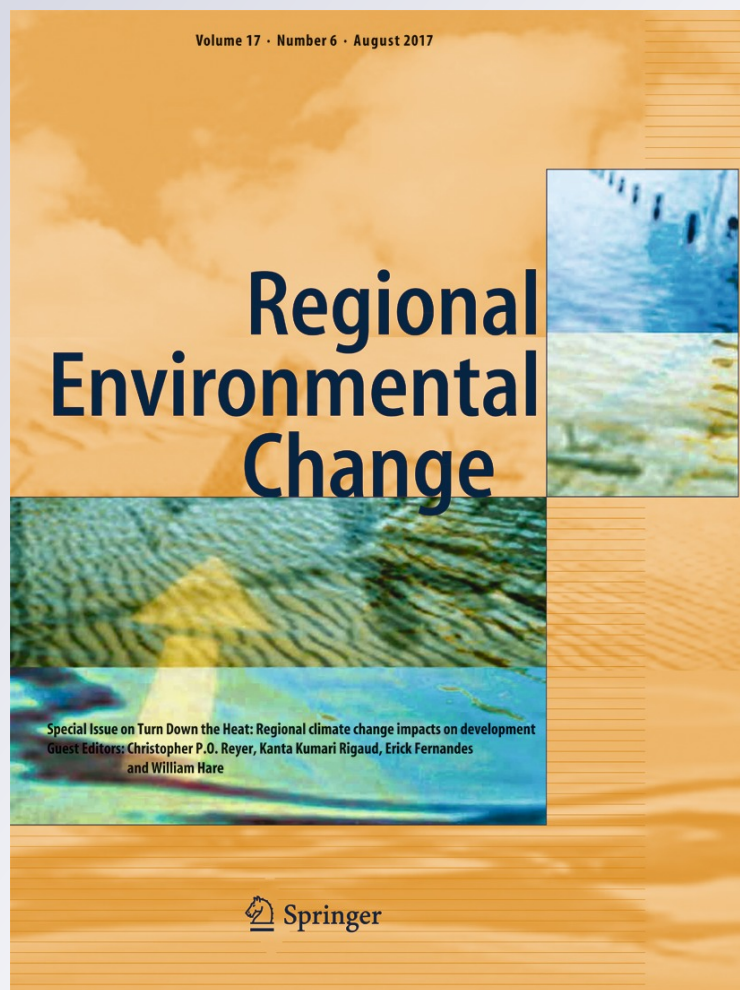
Volume 17

Number 6

Reg Environ Change (2017)

17:1853-1861

DOI 10.1007/s10113-017-1156-y



Your article is protected by copyright and all rights are held exclusively by Springer-Verlag Berlin Heidelberg. This e-offprint is for personal use only and shall not be self-archived in electronic repositories. If you wish to self-archive your article, please use the accepted manuscript version for posting on your own website. You may further deposit the accepted manuscript version in any repository, provided it is only made publicly available 12 months after official publication or later and provided acknowledgement is given to the original source of publication and a link is inserted to the published article on Springer's website. The link must be accompanied by the following text: "The final publication is available at link.springer.com".

Atmospheric drivers of sea-level fluctuations and nuisance floods along the mid-Atlantic coast of the USA

Scott C. Sheridan¹ · Douglas E. Pirhalla² · Cameron C. Lee¹ · Varis Ransibrahmanakul²

Received: 26 May 2016 / Accepted: 27 March 2017 / Published online: 24 April 2017
© Springer-Verlag Berlin Heidelberg 2017

Abstract As sea levels have risen and continue to rise, the risk of coastal flooding has increased in turn. While many studies have examined specific extreme flooding events, far fewer have explored the systematic associations between weather events and smaller, nuisance flood events. In this research, we take a synoptic climatological approach to assess this connection. We utilize self-organizing maps (SOMs) to separately cluster two atmospheric fields, sea-level pressure and 700-hPa geopotential height. We then utilize the output from these classifications to assess the impact of atmospheric conditions on the short-term fluctuations of sea level for the period 1979–2012, as well as the likelihood of nuisance flood occurrence, at five tidal gauges from Cape May, NJ, to Charleston, SC, along the mid-Atlantic coast of the USA. Results show the impacts of both the inverted barometer effect as well as surface wind forcing. Beyond this, the SOM nodes show a clear spatial continuum of associations between circulation and anomalous sea level, including some significant sea-level anomalies associated with relatively ambiguous pressure patterns. Moreover, the transitions from 1 day to the next are also analyzed, with results showing that rapidly deepening cyclones, or persistent onshore flow, can be associated with the greatest likelihood of nuisance floods. Results are generally weaker with 700-hPa height than sea-level pressure; however, in

some cases, it is clear that the mid-tropospheric circulation can modulate the connection between sea-level anomalies and surface circulation.

Keywords Self-organizing maps · Sea level · Nuisance flooding · Synoptic climatology · Climate change

Introduction

Changes in sea levels have been studied on many spatiotemporal levels, from the local to the global, from short-term to long-term, as well as secular trends. In terms of secular trends, there is ample evidence for a mean global sea-level rise of approximately 3 mm year⁻¹ over the last two decades (Church and White 2011). This rise has accelerated somewhat in recent decades, with interannual fluctuations that can be attributed to broader phenomena such as El Niño–Southern Oscillation (Cazenave et al. 2014), volcanic eruptions (Church and White 2011), melt from the Greenland ice sheet (van den Broeke et al. 2016), and variability in ocean circulation (Goddard et al. 2015). Phenomena that affect global mean temperatures will affect seasonal- to annual-level fluctuations in global mean sea level, with warm El Niño events leading to the greatest short-term global rise (Cazenave et al. 2014). On the regional scale, seasonal anomalies are observed in response to teleconnections, particularly the aforementioned El Niño, but also with other modes such as the North Atlantic Oscillation in the Mediterranean Sea and along the US East Coast (Landerer and Volkov 2013; Ezer and Atkinson 2014). The impacts of short-term atmospheric influences on sea levels has typically focused on the role of atmospheric pressure as the “inverted barometer” effect (Wunsch and Stammer 1997) and the role of atmospheric wind fields has been assessed in terms of modeling (Carrere and Lyard 2003). Frequency of storminess can be related to changes in sea level as well (Thompson et al. 2013).

Editor: James D. Ford

Electronic supplementary material The online version of this article (doi:10.1007/s10113-017-1156-y) contains supplementary material, which is available to authorized users.

✉ Scott C. Sheridan
ssherid1@kent.edu

¹ Department of Geography, Kent State University, Kent, OH, USA

² National Center for Coastal Ocean Science, NOAA, Silver Spring, MD, USA

In general, the most substantial impacts from short-term sea-level increases are coastal flooding events. These coastal flooding events must be modeled from the standpoint not just of changes in sea levels but also account for tidal variability and waves (Wolf 2009). Major coastal flooding events occur with the storm surges associated with tropical cyclones, such as the \$70 billion dollars in damage done by Hurricane/Cyclone Sandy in 2012 (NOAA 2013), and the impacts of such events is expected to increase further as background mean sea-level rises (Sweet and Park 2014). Beyond these well-studied, high-profile events, however, are a greater number of smaller-scale minor coastal flooding events, typically termed “nuisance flood” events in the USA (NOAA 2014). These events may be connected with more minor storms, or even persistent wind forcing, such as in the 2009 elevated sea levels across the East Coast of the USA (Sweet et al. 2009). Nuisance floods, especially when recurrent, may negatively affect coastal infrastructure in terms of stormwater drainage, road damage, and corrosion (NOAA 2014). Rising sea levels are also expected to contribute to beach or barrier island erosion (Irish et al. 2010). This degradation of natural and anthropogenic coastal defenses could lead to greater vulnerability during major events (Irish et al. 2010).

Nuisance floods are becoming increasingly common as sea-level increases (NOAA 2014). Nuisance flood definition levels vary spatially in terms of the specific elevation above mean higher high water (MHHW) level, as it is set to a level above which minor coastal flooding occurs. Thus, the number of exceedances per year varies from near 0 to near 40 across US coastlines, with areas along the mid-Atlantic coast relatively strongly affected. Heavy precipitation coinciding with these other atmospheric forcings can also augment impacts, particularly in low-lying deltas (Wolf 2009).

Multiple atmospheric drivers influence water-level variability and flooding along the mid-Atlantic coast. These include the direct effects of atmospheric pressure and circulation, wind stress and storm surge, wind-induced Ekman transport, and seasonal heating/cooling of the water column (Sweet et al. 2009, Woodworth et al. 2014). Strong northeasterly winds and elongated fetch associated with prevailing high pressure to the north can elevate coastal sea level via onshore flow and Ekman-driven convergence (Sweet et al. 2009). Likewise, strong onshore winds and fetch around low-pressure systems play a key role in storm surge, dynamic wave setup, and elevated mean sea levels above flood thresholds. Other factors known to influence water-level variability over seasonal to decadal time scales relate to ocean dynamics and spatial changes in Florida Current and Gulf Stream transport, where decreased transport and cross-current gradients can lessen the sea-level slope and increase sea level along the coast (Ezer 2015, Sweet 2009) with steepened gradients/slope having an opposite effect. In combination, these factors when superimposed on pre-existing tidal amplitudes and cycles can effectively result in a net movement of water onshore, changing local sea-level values to the point where flooding may occur.

Among these larger forces, the overall circulation of the atmosphere creates several key process-driven modes that influence the net movement of water onshore and water-level variability at a particular tide station. For example, in addition to the direct flooding impacts from tropical storms and hurricanes, the position and movement of mid-latitude cyclones/anticyclones and ultimate proximity to the coast reveal insights on the timing and persistence of wind patterns and sequences most critical to nuisance flood events. Through this work, we will dissect specific interactions and components of atmospheric circulation to uncover these critical attributes to nuisance flooding along the East Coast.

Given the increasing frequency of coastal flooding, and projected changing atmospheric circulation patterns (e.g., Sheridan et al. 2012) and further rise in sea-level (e.g., DeConto and Pollard 2016), examining the link between atmospheric circulation and flooding events can illuminate broader-scale connections between the two and potentially assist in short-term forecasting and long-term adaptation. One way of assessing atmospheric circulation variability is via synoptic climatological methods, in which atmospheric patterns are classified into one of a number of groups based on similarities (Yarnal 1993). In particular, self-organizing maps (SOMs), in which patterns are arrayed in a multi-dimensional continuum (Sheridan and Lee 2011), can provide excellent visualization of circulation variability and its connection to environmental conditions. Synoptic categorizations can capture not only short-term changes in sea level, by virtue of their inherent incorporation of atmospheric pressure and wind fields, but also allow inference of wave activity and precipitation as well. Synoptic methods have scarcely been used to systematically analyze coastal flooding. Only one known study employed SOMs: Izaguirre et al. (2012) used the method to cluster monthly mean sea-level pressure fields in the North Atlantic in order to examine extreme wave heights in the region.

Here, we use the SOM technique to separately cluster two atmospheric fields, sea-level pressure and 700-hPa geopotential height, for use in identifying the impact of atmospheric conditions on the short-term fluctuations of sea level at five tidal gauges from Cape May, NJ, to Charleston, SC, along the mid-Atlantic coast of the USA. The likelihood of coastal nuisance flooding, as defined by NOAA, associated with synoptic circulation patterns is also assessed, both for the entire period 1979–2012, as well as the long-term trends in the likelihood of a nuisance flood given the background sea-level rise.

Data and methods

Data sets and the creation of self-organizing maps

Daily mean sea-level pressure (SLP) and daily mean 700-hPa geopotential height (Z700) data were obtained from the North American Regional Reanalysis (NARR; Mesinger et al. 2006)

project website for the period 1979–2014 for each available grid point within the domain of 50° N to 27.5° N latitude and 90° W to 60° W longitude. Prior to SOM analysis, each of these two data sets were organized into separate matrices consisting of 13,149 rows (days) and 6461 columns (spatial grid points at 32 km resolution) and transformed into z scores on a column-by-column basis. Each z score matrix was then subjected to an unrotated, s -mode principal components analysis (PCA) to reduce data dimensionality and initialize the subsequent SOMs based upon the leading principal components (PCs). The PC scores of the PCs with eigenvalues greater than 1 in each data set were retained, yielding 27 PCs for the SLP data (accounting for 99.8% of the variance in the SLP data set) and 19 PCs for the Z700 data (accounting for 99.9% of the variance in the Z700 data set). These retained PCs were directly used in the SOM-based classification.

Self-organizing maps were constructed using custom scripts in the Neural Network Toolbox in MATLAB R2015b. Separate SOMs were constructed from the retained principal component scores in each data set using the following custom settings: a 7×5 structure, the “gridtop” topology, the “boxdist” distance function, the incremental (“learnsom”) learning function and 1000 iterations. The initial neighborhood distance is automatically set to the maximum distance between neurons, 6 (based upon the SOM size, topology, and distance function) and decreases to 1 throughout training, and the learning rate parameters were left at their default settings (starting at 0.9 and incrementally decreasing to 0.02 throughout training). The choice of a 7×5 SOM was based upon previous literature examining SLP variability near the East Coast of the USA (Hewitson and Crane 2002, Crane and Hewitson 2003). Thus, the resulting SOM for each of the data sets contains 35 nodes (Figs. 1 and A1); the Sammon maps (displaying the distances between all neurons in SOM-space) are displayed in Figs. A2 and A3.

Tidal gauge data were obtained from the NOAA Center for Operational Oceanographic Products and Services (CO-OPS; <http://tidesandcurrents.noaa.gov>) for five stations (Table A1, Fig. 2) for the period 1979–2012. Hourly data, along with daily mean water-level data, relative to the National Tidal Datum Epoch, were both obtained (NOAA 2014). Prior to analysis of average sea level by SOM node, the long-term linear trend (Table A1) in daily tidal gauge data was subtracted to create an anomalous daily mean sea level (ASL) for each day. Hourly tidal gauge data were used to calculate the incidence of a nuisance flood on a given day (defining a flood as at least 1 h in exceedance of the flood level).

Anomalous sea-level values and identification of flood events

Mean anomalous detrended sea-levels (ASL) on all days that each SOM-based nodes occurred between 1979 and 2012

were calculated, along with standard deviation and the total number of occurrences. Two-tailed one-sample difference of means t tests were computed to assess whether each of these means were significantly ($p < 0.05$) different from zero (due to them being anomalies). Due to a high degree of temporal autocorrelation in the sea-level values, an “effective sample size” was computed for the calculation of the t statistic and for determining the degrees of freedom when calculating the p value, using the following equation derived from Wilks (2006):

$$N' = N \left(\frac{1-r}{1+r} \right)$$

where N' is the effective sample size, N is the actual observed sample size and r is the lag-1 serial correlation for the entire time series.

Nuisance floods are defined as days on which the observed sea level is above nuisance threshold criteria for at least 1 h, as set by the local National Weather Service (Table A1). Because of the long-term trend in mean sea level, nuisance flood likelihood has increased substantially over recent decades (NOAA 2014). To assess the influence of atmospheric patterns on floods irrespective of background sea-level rise, sea-level values were all “raised” to 2012 levels, by adding the difference between sea level on each day and at the end of the record (based on a linear trend line for each station for the 1979–2012 period); an example for Cape May is depicted in Fig. A4.

Results and discussion

Self-organizing maps

The SOM produced using mean daily sea-level pressure data shows a smooth continuum of SLP fields (Fig. 1), with high-pressure dominant patterns in the lower right-hand corner (node 7), transitioning to lower-pressure dominant patterns in the upper left-hand corner (node 29), and the other two corners, nodes 1 and 35, containing similar pressure gradients.¹ Weak pressure patterns tend to dominate the middle of the SOM. Several pressure features can be seen to transcend the nodes. The high-pressure centers include manifestations of both the Bermuda High (e.g., nodes 1, 2, 27, 28, and 35) and a

¹ Relative levels of similarity across the SOM nodes can be seen via a Sammon map (Figure A2), where nodes 7 and 29 are most dissimilar but nodes 1 and 35 curve back around. The folded Sammon map is due to the fact that the shape of the multi-dimensional data cloud is impacted substantially by the variance within the third dimension of the SOM data space (represented herein as the third PC), and folding allows this variability to be incorporated into the SOM. Due to this curviness of the Sammon map, the representative SLP patterns (node 1 and node 35) share a similar spatial pattern, with slight differences in the magnitudes of the lowest and highest pressure centers in each.

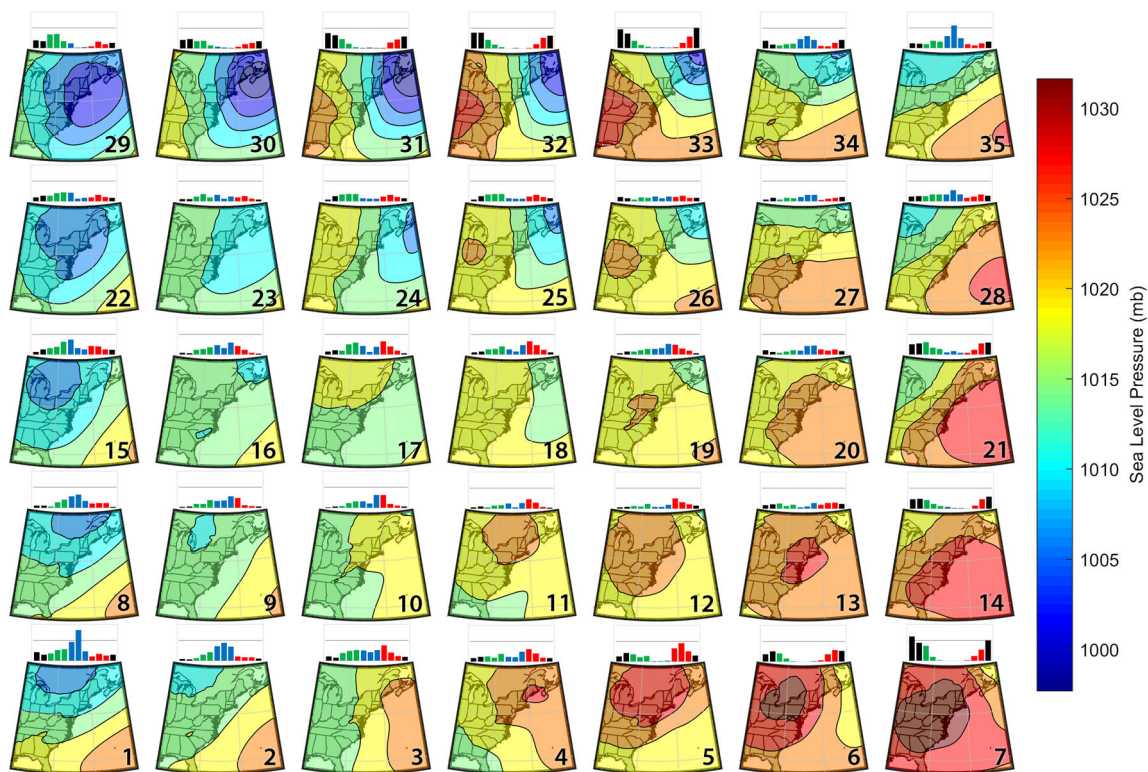


Fig. 1 Self-organizing map produced with sea-level pressure data for the study region. Node numbers are indicated in the lower right-hand corner of each map. Monthly frequency of each node is indicated by the bars

above each map, color coded by season (winter = black, spring = green, summer = blue, autumn = red). Gray line indicates 10% of all days

continental high (e.g., nodes 6, 7, and 14). Strong low-pressure centers are mostly centered on the mid-Atlantic coast or northeastward (e.g., nodes 29–33). The mean annual frequencies of the SLP nodes are relatively equal, with each node present on between 2 and 4% of all days, except for node 1 (5.2%). Most nodes have seasonal variability in their occurrence; the very strong coastal lows tend to predominate in the cold season, as do the continental highs, whereas the Bermuda High patterns tend to occur most frequently in summer. As is typical of the middle latitudes, the transitional seasons feature a wider variety of patterns, though only a few nodes are transitional season dominant (e.g., nodes 5 and 17).

Unlike with sea-level pressure, 700-hPa geopotential heights vary substantially by season, and hence seasonal affiliation dominates the spatial distribution of Z700 nodes (Fig. A1; Sammon map in Fig. A3), with warmer season patterns on the left and colder season patterns on the right. Across the nodes, variability is seen in the trough axis, from over the Atlantic in node 5, to along the coast in node 7, to over the Ohio River Valley in node 21, and trough magnitude, as troughs generally become more amplified towards the bottom of the matrix. Thermal gradients generally get weaker moving towards the left. Mean annual frequencies of the Z700 nodes are also relatively equally distributed, with only the weak-flow Bermuda high node 29, at 8%, outside of the 2 to 4% range. As all nodes have very strong seasonality, they all effectively

disappear for portions of the year. The seasonality is strongest in the upper left and lower right corners, where the Bermuda High and strong coastal troughs are effectively entirely limited to the summer and winter months, respectively.

The association between atmospheric patterns and anomalous sea levels

Sea-level pressure (SLP) patterns exert a substantial influence on anomalous sea-level values and likelihood of nuisance flooding (Table 1). Statistically significant elevated sea levels are observed in a continuous swath extending from node 29 down through node 5. These nodes comprise a number of different weather situations, ranging from a broad coastal low-pressure system (node 29), in which the inverted barometer effect is prevalent, to high-pressure centers anchored to the north of the study region (nodes 4, 5, and 11), in which northeasterly winds would generate onshore flow. Interestingly, elevated sea levels are also observed with more ambiguous pressure patterns in between (e.g., node 17), hinting at a synergistic relationship between persistent high-pressure patterns to the north and developing low pressure to the south over consecutive days. Below-normal sea levels tend to occur with the converse situations, strong high pressure (e.g., node 7) as well as offshore flow (nodes 1 and 35). This pattern of sea-level response across SOM-space is

Fig. 2 The 5 tidal gauge stations used in this research



generally geographically cohesive, with the exception of the southernmost station, Charleston, which is farther from the key pressure centers.

The overall likelihood of nuisance flooding varies substantially across stations, with likelihoods greater at Cape May, Lewes, and Charleston where the flood level benchmarks are lower (Table A1). The variability in flood likelihood by pressure pattern strongly correlates with the mean daily sea-level anomalies, although in Cape May and Lewes in particular, there are somewhat greater relative likelihoods of flood events in strong low-pressure situations (e.g., node 29) than in onshore flow situations, while no general distinction is observed in Charleston.

The 700-hPa geopotential height patterns (Z_{700}) are associated with fewer statistically significant correlations with sea level at all stations, other than Charleston (Table A2). Once again, the patterns associated with increased water levels

appear in a continuum (in this case, spread across the center of the matrix), generally associated with advancing troughs, along with advancing ridges in nodes 1 and 8, which commonly would be associated with high pressure along the northeast coast, and onshore flow. Lower than normal water levels are generally only connected with cold season dominant patterns in which a very strong pressure gradient exists (nodes 32–35), and also along the deeper troughs on the right side of the matrix at Charleston. While the likelihood of nuisance flooding is again in line with sea-level anomalies, the distinction is less substantial from node to node.

The influence of atmospheric pattern transitions on anomalous sea levels

As shown above, short-term anomalies in sea levels can be associated with atmospheric patterns occurring on the same

Table 1 Mean daily sea-level anomalies (left) and probability of nuisance flood using sea-levels adjusted to 2012 levels (right) by SLP SOM node. For the anomalies, blue (orange) highlights indicate statistically significant ($p < 0.05$) increases (decreases) in sea level. For the flooding likelihood, values are shaded by value relative to overall mean for each station

Anomalous sea-level (mm)							Probability of nuisance flood (%)						
Cape May													
137	19	-47	-108	-170	-71	-61	27	13	7	3	1	5	5
100	109	69	-4	-30	-71	-51	19	19	15	9	7	2	5
88	89	129	58	-8	-28	-99	16	13	21	13	5	5	3
18	55	81	97	19	-51	-135	9	16	14	19	5	4	2
-33	12	55	79	97	-41	-174	4	12	10	16	16	6	2
Lewes													
137	11	-72	-126	-189	-78	-68	23	9	3	2	1	2	2
100	118	79	3	-27	-75	-55	12	14	11	4	3	0	2
83	94	145	69	-4	-27	-106	8	7	15	10	1	2	1
14	54	91	112	26	-49	-145	4	6	8	14	3	1	1
-41	13	63	101	123	-29	-175	2	5	7	12	14	4	0
Chesapeake													
117	46	-22	-68	-131	-93	-98	5	2	0	0	0	0	0
75	112	90	18	-25	-89	-86	2	4	2	0	0	0	0
44	83	150	79	0	-33	-131	0	2	4	1	0	0	0
-16	36	90	136	48	-37	-149	0	0	1	4	0	0	0
-78	-13	44	113	165	7	-146	0	0	1	3	6	2	0
Duck													
114	62	16	-29	-112	-101	-111	7	3	2	1	0	0	0
58	109	95	29	-24	-90	-100	2	5	4	2	0	0	0
25	73	141	81	6	-35	-134	0	1	8	3	1	0	0
-29	27	83	134	59	-26	-143	0	0	1	8	1	0	0
-96	-25	24	97	161	21	-125	0	0	0	4	9	2	0
Charleston													
-66	-68	-92	-83	-107	-87	-65	5	5	4	3	1	2	3
-23	34	44	2	-15	-41	-34	8	8	10	6	5	5	5
-12	57	98	84	46	22	-34	7	9	14	14	7	8	5
-35	40	85	139	101	51	-34	6	13	13	20	17	11	4
-94	-10	43	111	152	43	-37	3	7	9	15	18	9	6

day, particularly with SLP. However, a more nuanced understanding of anomalous sea levels and nuisance flooding can be seen by evaluating how sea level relates to weather conditions on the day preceding as well, thus evaluating the response to transitions or sequences of atmospheric patterns. Six different broad categories of transitions can be associated with

increased sea levels, including both sharp transitions as well as persistent patterns (Fig. 3, Table A3). The greatest positive anomalies across the four northern stations are observed with several different *deepening cyclone* transitions (A in Fig. 3), most spanning a jump of two nodes towards the upper left of the SOM matrix. These transitions, occurring predominately

between September and April, broadly represent patterns in which high pressure is prominent to the north, with northeasterly/easterly winds and Ekman-induced convergence along the coast, concurrent with, low pressure centered over the Carolinas, promoting a strong easterly fetch, and storm surge, thereby compounding increases in sea level and leading to the greatest likelihood of flooding; some individual transition pairs have a greater than 50% likelihood of coastal flooding at Cape May and Lewes (Table A3). As the core of the pressure center moves north of the coastal sites, the

response generally decreases southward and is ambiguous at Charleston. *Transitioning cyclone* situations (Fig. 3, B)), in which low pressure is already in place, and *decreasing pressure* transitions (Fig. 3, C), of similar direction to (A) but lower on the matrix and generally lesser in magnitude, also lead to increased sea levels on average, but to a lesser extent and are thus less likely to lead to nuisance flooding.

Several combinations of anticyclonic patterns, nonsynchronous with deepening cyclone patterns occurring most frequently in autumn and secondarily in spring, are also

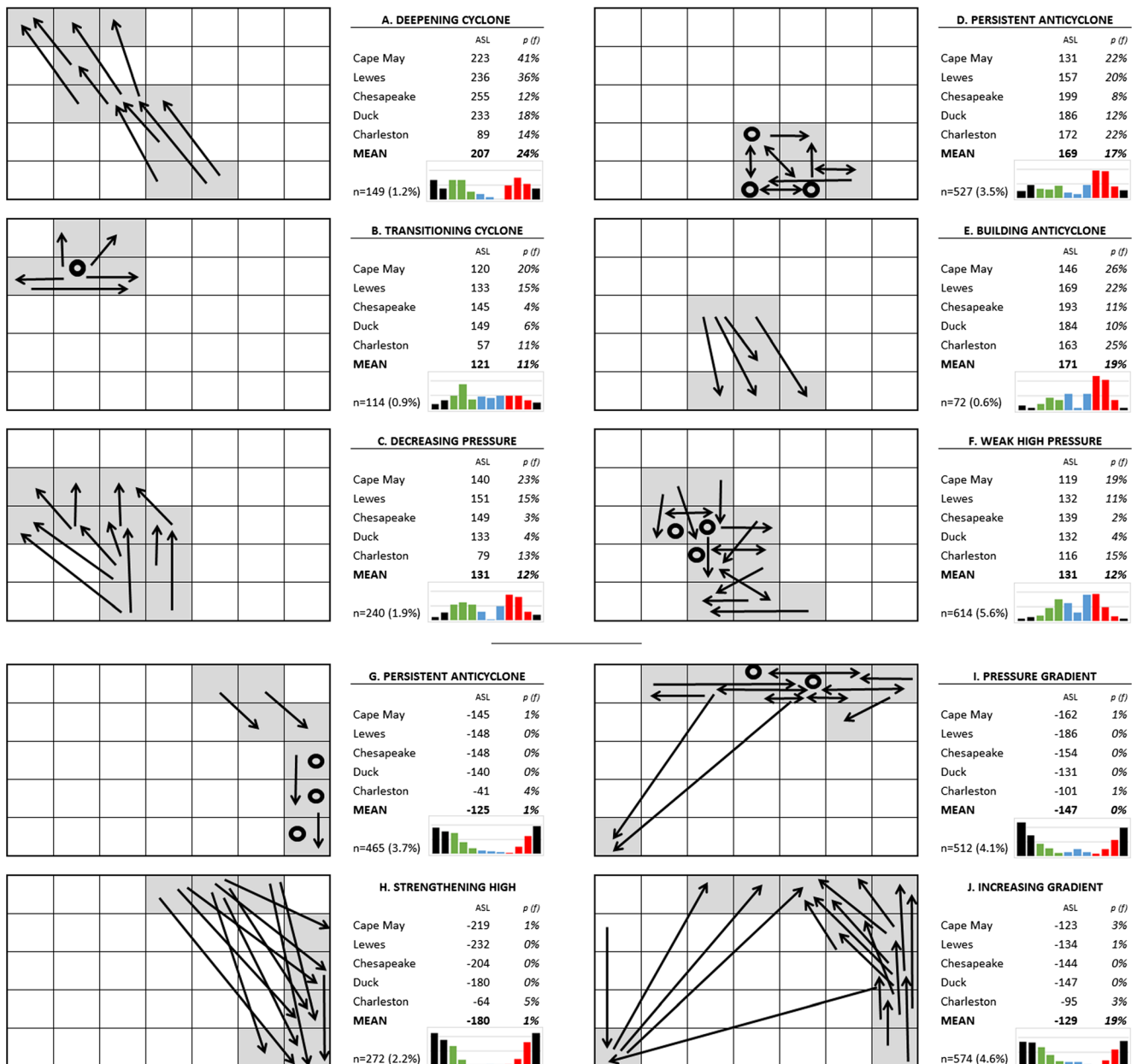


Fig. 3 Schematic of main SLP node transition groups associated with anomalously high and low sea levels, with the mean anomalous sea-level (ASL) and probability of flooding ($p(f)$) for each group. *Arrows* represent transition from day before anomalous water event to day of event; *circles* represent a pattern repeating on both days. All transitions with $n > 10$

and a mean sea-level anomaly of ± 100 mm across all 5 stations are represented. Monthly frequency of each transition group is indicated by the *bars* above each map, color coded by season (winter = black, spring = green, summer = blue, autumn = red). *Gray line* indicates 10% of all days

associated with increased flood likelihood. In contrast with the cyclonic patterns above, these affect all five sites similarly. *Persistent anticyclones (D)*, centered broadly over the St. Lawrence Valley (nodes 4–6 and 11–12), and to a lesser extent, *weak high pressure transitions (F)*, are associated with elevated sea levels and increased flooding. While the least common, *building anticyclone transitions (E)* are likely associated with increasing onshore flow and hence the greatest increases in sea level seen among anticyclonic situations, and thus a greater likelihood of flooding.

Four sets of transitions can also be identified that lead to decreased sea levels, and a near-zero likelihood of nuisance flooding. These patterns, in comparison to the increased sea-level patterns, predominately occur between November and March. *Persistent high (G)* and *Strengthening high (H)* transitions both lead to decreased sea levels across the northern four stations and are likely a function of the inverted barometer influence as these nodes are associated with the highest SLP. *Pressure gradient (I)* and *Increasing gradient (J)* both are associated with either consistent or increasing offshore flow across all sites.

In contrast with the SLP transitions, fewer Z700 transition patterns can be associated with highly anomalous sea levels, and the relationships are generally weaker and more ambiguous (Fig. A5, Table A4). Increased sea levels can be associated with two distinct types of transitions. Persistent or developing *coastal troughs (A)*, of varying gradients and amplitudes, occupying the lower center of the SOM matrix, are generally associated with increased sea levels, particularly farther north. *Developing ridge patterns (B)*, particularly associated with node 1, are associated with increased sea level, particularly towards the south, with a 26% likelihood of nuisance flooding at Charleston. Both sets of transitions are transitional season dominant, though coastal troughs tend to occur towards the colder months (peaking in April and November) while the ridges peak in May and September.

Decreased sea levels are associated with two types of Z700 transitions, both of which have a strong winter dominance. *Strong gradient (C)* is associated with the strong geostrophic flow patterns aligned on the right side of the SOM matrix, while *building ridge (D)* is a combination of several transitions that broadly include a strong gradient lessening and/or migrating eastward.

The interaction between atmospheric patterns at Z700 and SLP on anomalous sea levels

While SLP is generally more closely associated with sea levels, the interplay between SLP circulation and circulation at Z700 can also be explored. Using a sample of subsets (Table A5), the relative importance of mid-tropospheric circulation in modulating the SLP-to-sea level relationship is evident. At Cape May and Charleston, the greatest positive

anomalies are associated with the low-pressure center SLP node 29 and the broad continental high SLP node 5, respectively. Subdividing sea-level response by Z700 node, relatively weak gradient flows in Z700 nodes 12 and 13 are associated with higher sea levels at Cape May than the stronger gradients that surround it, particularly Z700 nodes 7, 14, and 21. While somewhat less geographically cohesive, at Charleston SLP node 5 is generally associated with higher sea levels when Z700 nodes with a moderate trough axis inland and smaller increases in sea level when the pressure gradient is greater.

As mentioned in “The association between atmospheric patterns and anomalous sea levels” section, the weak/developing low-pressure pattern SLP node 17 is associated with increased sea levels at all sites. Segregating the response by Z700 node, some further clarity can be seen in that the greatest increases in sea level can be observed with the spring dominant troughs in Z700 nodes 18 and 19, as well as Z700 node 1—a high amplitude ridge along the northeast coast. Lesser sea-level increases are concentrated with patterns with the greatest geopotential heights, Z700 nodes 15 and 16.

Conclusions

The results presented above show manifestations of some well-established factors in terms of short-term changes of sea level, namely, the inverted barometer effect as is manifested in the surface pressure patterns and surface wind forcing as is depicted in the relative cyclonicity of the pressure fields. Beyond this, a clear continuum of sea-level associations can be seen in the results of the SLP SOM matrix, including positive sea-level deviations associated with some ambiguous pressure patterns (e.g., node 17) that are aligned in between the low-pressure centers such as node 29 and the onshore flow in node 5. Analysis of the pattern transitions suggest that rapidly deepening cyclones, or persistent onshore flow, can be associated with the greatest likelihood of nuisance floods. Under this scenario, strong high pressure to the north would initiate onshore flow due to persistent northeasterly/easterly winds and Ekman-induced transport, concurrent with a stationary or oscillating low pressure to the south creating added surge and perhaps hinting at dual mechanisms related to these transitional situations. Nodes 11 and 17 show remnants of a continental high setup to support this idea. Results are somewhat weaker for Z700 nodes, with fewer clear associations and in general a lesser stratification of flood likelihood. Nevertheless, transitions, particularly those across multiple nodes, can be readily associated with anomalous sea levels. Moreover, it is clear that the mid-tropospheric circulation can modulate the SLP—sea-level association.

The SOM model has shown that it can be used to understand the general association between atmospheric circulation and short-term fluctuations in sea level. In the long term, these

relationships may be extrapolated for use in combination with global climate models to assess changes to atmospheric circulation pattern frequency, persistence, and sequencing that may well impact the future frequency and magnitude of nuisance flood events, especially as the shoreline continues to recede in response to climate change, and tipping points of frequent coastal flooding are likely reached (Sweet and Park 2014). In the short term, this methodology could be used to develop circulation-driven models that produce seasonal- to monthly-scale outlooks of water level changes, including both low-water and flooding events, providing ample warning to vulnerable areas and improving overall coastal intelligence in ecologically and economically important coastal environments.

Acknowledgments We thank the personnel at the Center for Operational Oceanographic Products and Services for making the sea level and tide gauge data products available; University of Hawaii Sea Level Center for providing consistent sea-level time series; and NOAA's Earth System Research Laboratory, Physical Sciences Division, for providing up-to-date gridded NCEP North American Regional Reanalysis products. Funding support for the study was provided by NOAA's National Center for Coastal Ocean Science, as part of a 2-year climate impacts project (L8K5NCC-PCL) to address coastal ecosystem impacts of threshold events. We also thank the Editor-in-Chief and two anonymous reviewers for their helpful comments that improved this manuscript.

References

- Carrere L, Lyard F (2003) Modeling the barotropic response of the global ocean to atmospheric wind and pressure forcing-comparisons with observations. *Geophys Res Lett* 30:1275. doi:10.1029/2002GL016473
- Cazenave A, Dieng HB, Meyssignac B, von Schuckmann K, Decharme B, Berthier E (2014) The rate of sea-level rise. *Nature Clim Change* 4(5):358–361. doi:10.1038/nclimate2159
- Church JA, White NJ (2011) Sea-level rise from the late 19th to the early 21st century. *Surv Geophys* 32(4–5):585–602. doi:10.1007/s10712-011-9119-1
- Crane RG, Hewitson BC (2003) Clustering and upscaling of station precipitation records to regional patterns using self-organizing maps (SOMs). *Clim Res* 25:95–107. doi:10.3354/cr025095
- DeConto RM, Pollard D (2016) Contribution of Antarctica to past and future sea-level rise. *Nature* 531(7596):591–597. doi:10.1038/nature17145
- Ezer T (2015) Detecting changes in the transport of the Gulf Stream and the Atlantic overturning circulation from coastal sea level data: the extreme decline in 2009–2010 and estimated variations for 1935–2012. *Glob Planet Chang* 129:23–36. doi:10.1016/j.gloplacha.2015.03.002
- Ezer T, Atkinson LP (2014) Accelerated flooding along the U.S. East Coast: on the impact of sea-level rise, tides, storms, the Gulf Stream, and the North Atlantic Oscillations. *Earth's Future* 2(8):362–382. doi:10.1002/2014EF000252
- Goddard PB, Yin J, Griffies SM, Zhang S (2015) An extreme event of sea-level rise along the northeast coast of North America in 2009–2010. *Nat Commun* 6:6346. doi:10.1038/ncomms7346
- Hewitson BC, Crane RG (2002) Self-organizing maps: applications to synoptic climatology. *Clim Res* 22:13–26. doi:10.3354/cr022013
- Irish JL, Frey AE, Rosati JD, Olivera F, Dunkin LM, Kaihatu JM, Ferreira CM, Edge BL (2010) Potential implications of global warming and barrier island degradation on future hurricane inundation, property damages, and population impacted. *Ocean Coastal Manag* 53(10):645–657. doi:10.1016/j.ocecoaman.2010.08.001
- Izaguirre C, Menéndez M, Camus P, Méndez FJ, Mínguez R, Losada JJ (2012) Exploring the interannual variability of extreme wave climate in the Northeast Atlantic Ocean. *Ocean Modell* 59:31–40. doi:10.1016/j.ocemod.2012.09.007
- Landerer FW, Volkov DL (2013) The anatomy of recent large sea level fluctuations in the Mediterranean Sea. *Geophys Res Lett* 40(3):553–557. doi:10.1002/grl.50140
- Mesinger F, DiMego G, Kalnay E, Mitchell K, Shafran PC, Ebisuzaki W, Jovic D, Woollen J, Rogers E, Berbery EH, Ek MB (2006) North American regional reanalysis. *Bull Amer Meteorol Soc* 87(3):343–360. doi:10.1175/BAMS-87-3-343
- National Weather Service Service Assessment NOAA (2013) Service assessment: hurricane/post-tropical cyclone Sandy—October 22–29 2012. Silver Spring, MD, 46pp
- NOAA (2014) Sea level rise and nuisance flood frequency changes around the United States. NOAA Technical Report NOS CO-OPS 073, 66 pp
- Sheridan SC, Lee CC (2011) The self-organizing map in synoptic climatological research. *Prog Phys Geogr* 35(1):109–119. doi:10.1177/0309133310397582
- Sheridan SC, Lee CC, Allen MJ, Kalkstein LS (2012) Future heat vulnerability in California part I: projecting future weather types and heat events. *Climat Change* 115:291–309. doi:10.1007/s10584-012-0436-2
- Sweet WV, Park J (2014) From the extreme to the mean: acceleration and tipping points of coastal inundation from sea level rise. *Earth's Future* 2(12):579–600. doi:10.1002/2014EF000272
- Sweet WV, Zervas C, Gill S (2009) Elevated east coast sea levels anomaly: July–June 2009. NOAA Technical Report NOS CO-OPS 051, 40 pp
- Thompson PR, Mitchum GT, Vonesh C, Li J (2013) Variability of winter storminess in the eastern United States during the twentieth century from tide gauges. *J Clim* 26(23):9713–9726. doi:10.1175/JCLI-D-12-00561.1
- Van den Broeke MR, Enerlin EM, Howat IM, Kuipers Munneke P, Noel BPY, van de Berg WJ, van Meijgaard E, Wouters B (2016) On the recent contribution of the Greenland ice sheet to sea level change. *Cryosphere* 10:1933–1946. doi:10.5194/tc-10-1933-2016
- Wilks DS (2006) *Statistical methods in the atmospheric sciences*, Second edn. Academic Press, Elsevier, Burlington
- Woodworth PL, Maqueda M, Roussenov MÁ, Williams VM, Hughes RG (2014) Mean sea level variability along the northeast American Atlantic coast, and the roles of the wind and the overturning circulation. *J Geophys Res Oceans* 119:8916–8935. doi:10.1002/2014JC010520
- Wunsch C, Stammer D (1997) Atmospheric loading and the oceanic “inverted barometer” effect. *Rev Geophys* 35(1):79–107. doi:10.1029/96RG03037
- Wolf J (2009) Coastal flooding: impacts of coupled wave–surge–tide models. *Nat Haz* 49(2):241–260. doi:10.1007/s11069-008-9316-5
- Yarnal B (1993) *Synoptic climatology in environmental analysis: a primer*. Belhaven press, London